Journal Pre-proof

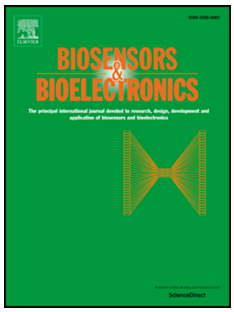

A wearable battery-free wireless and skin-interfaced microfluidics integrated electrochemical sensing patch for on-site biomarkers monitoring in human perspiration

Shipeng Zhang, Md. Abu Zahed, Md. Sharifuzzaman, Sanghyuk Yoon, Xue Hui, Sharat Chandra Barman, Sudeep Sharma, Hyo Sang Yoon, Chani Park, Jae Yeong Park

PII: S0956-5663(20)30830-7

DOI: https://doi.org/10.1016/j.bios.2020.112844

Reference: BIOS 112844

To appear in: *Biosensors and Bioelectronics*

Received Date: 14 September 2020

Revised Date: 6 November 2020

Accepted Date: 20 November 2020

Please cite this article as: Zhang, S., Zahed, M.A., Sharifuzzaman, M., Yoon, S., Hui, X., Chandra Barman, S., Sharma, S., Yoon, H.S., Park, C., Park, J.Y., A wearable battery-free wireless and skin-interfaced microfluidics integrated electrochemical sensing patch for on-site biomarkers monitoring in human perspiration, *Biosensors and Bioelectronics* (2020), doi: https://doi.org/10.1016/j.bios.2020.112844.

CRediT Author Statement:

Shipeng Zhang: Conceptualization, Formal analysis, Writing – original draft, Validation. **Md. Abu Zahed:** Investigation, Experimental analysis, & Editing. **Md. Sharifuzzaman:** Visualization, Writing – original draft, & Editing. **Sanghyuk Yoon:** Methodology. **Xue Hui:** Methodology. **Sharat Chandra Barman:** Writing – review & editing. **Sudeep Sharma:** Review & editing. **Hyo Sang Yoon:** Formal analysis, Methodology. **Chani Park:** Methodology. **Jae Yeong Park:** Funding acquisition, Supervision.

A wearable battery-free wireless and skin-interfaced microfluidics integrated electrochemical sensing patch for on-site biomarkers monitoring in human perspiration

*Shipeng Zhang, Md. Abu Zahed, Md. Sharifuzzaman, Sanghyuk Yoon, Xue Hui, Sharat Chandra Barman, Sudeep Sharma, Hyo Sang Yoon, Chani Park, and Jae Yeong Park **

Department of Electronic Engineering, Kwangwoon University, 447-1 Wolgye-dong, Nowongu, Seoul 01897, Republic of Korea.

Corresponding author e-mail: jaepark@kw.ac.kr (Jae Yeong Park)

Abstract

In this study, an ultra-high sensitive, flexible, wireless, battery-free, and fully integrated (no external analysis equipment) electrochemical sensing patch system, including a microfluidic-sweat collecting unit, was newly developed for the on-site monitoring of the [K^+] concentration in human sweat. Multiwalled carbon nanotube (MWCNT) and MXene-$Ti_3C_2T_X$ based hybrid multi-dimensional networks were applied to obtain a high surface activation area and faster charge transfer rate, strongly adsorbing the valinomycin membrane to protect the ionophore for effective transshipment and immobilization of the [K^+]. Furthermore, the controllable porosity of carbon-based materials can accelerate the kinetic process of ion diffusion. This hybrid nanonetwork structure effectively enhanced electrochemical stability and sensitivity, addressing the noise and signal drifting problems experienced with low concentration detection. The fabricated sensor exhibited a high ion concentration sensitivity of 63 mV/dec with excellent selectivity, amplified to 173 mV/dec with the integrated amplification system. The Near Field Communication (NFC) is used to transmit measurements to a smartphone wirelessly. A microfluidic channel was integrated with the electrochemical sensor patch to efficiently collect sweat on the human skin surface and mitigate the sensor surface contamination problem.

Furthermore, the developed sensing patch can also be applied to other biomarkers on-site detection after modifying the working electrode with the corresponding selective membranes.

Keywords: MXene-MWCNTs, wireless RF energy harvesting, battery-free, microfluidics integrated, flexible biosensor, human perspiration

1. Introduction

Wearable biosensing devices have a broad impact on our daily lives, especially in the promising medical field, because of their ability to provide continuous, non-invasive, and real-time monitoring of physiological biomarkers in body fluids. But there are still many problems to be solved for the success of large-scale commercialization. Ensuring the accurate and reliable response of wearable biosensors is crucial to their market acceptance. The accuracy of wearable biosensors is often affected by surface contamination, which is the main factor limiting the continuous operation of sensors. (Shiwaku et al., 2018) Robust anti-fouling surface protection is necessary to ensure the reliability of sensors for the long-term. Another essential functional requirement for wearable devices is to maintain low power consumption during continuous monitoring, to provide useful and timely information to the wearer or other end users. The most common method of powering wearable biosensors involves using lithium-ion or alkaline batteries. However, such batteries are bulky and can cause toxicity problems, especially in lithium-ion-based systems. (Gao et al., 2016)

Recently, attention has focused on using wearable biosensors for measuring biomarkers in body fluids to reflect the physiological state of the body. These biomarkers are widely found in sweat, tears, and saliva in human body fluids. (Sonner et al., 2015; Villiger et al., 2018) Human sweat is a surprisingly biomarker-rich fluid that is gaining increasing attention. Therefore, this study

analyzed human sweat to detect the concentration of potassium ions [K^+]. [K^+] plays an essential role in maintaining the balance of body fluids and regulating body functions. The normal range of [K^+] concentration in human sweat is 4 to 24 mM. (Sonner et al., 2018) Abnormal [K^+] concentration levels can cause numerous health problems or diseases. A severe shortage of [K^+] in body fluids may cause a potentially fatal condition known as hypokalemia. Excess [K^+] may increase the risk of high blood pressure and strokes. (Fan et al., 2012; Teixeira et al., 2009; Viera and Wouk, 2015) Measuring the [K^+] losses from athletes' sweat could help health professionals plan personalized water and electrolyte replacement strategies to prevent water/electrolyte imbalances and heat-related whole-body muscle cramps in sports that could impair athletic performance. (Baker et al., 2014; Barnes et al., 2019) Therefore, the effective detection of physiological [K^+] concentrations is very significant in the healthcare field. (Yuan et al., 2019) More importantly, previous studies of [K^+] sensors have shown that low electrical conductivity in the transfer layer leads to slow response times and low electrical sensitivity (Bobacka et al., 1999; Yoon et al., 2020; Zeng and Qin, 2017) while also seriously affecting the accuracy of the measurement results. Previous studies involving the detection of low [K^+] concentrations also identified significant noise and signal drift issues. (Shiwaku et al., 2018) In such cases, the electrode material used could not effectively immobilize the ionophore in the membrane. Therefore, there is an urgent requirement for developing new materials to improve [K^+] concentration measurement's accuracy and sensitivity.

This study proposed a novel type of all-solid-state [K^+] ion-selective electrode based on a hybrid MXene-$Ti_3C_2T_X$ and multiwalled nanotube (MWCNTs) network structure, and this hybrid nano-network structured material was first used as an electrode transfer layer to measure the concentration of [K^+] in human sweat. The proposed MWCNTs and MXene-$Ti_3C_2T_X$ hybrid

working electrode were fabricated on the top of the screen-printed carbon paste on a polyethylene terephthalate (PET) substrate using a layer-by-layer deposition technique. The MXene-$Ti_3C_2T_X$, which displays a two-dimensional (2D) layer structure, provides outstanding electrical conductivity and a large surface area. Unfortunately, as the pulverized individual MXene-$Ti_3C_2T_X$ sheets are discrete distribution and agglomerated easily, they can impede ion transport, resulting in a lower conductance of the electrode surface and a significant loss of surface reactivity. (Orangi et al., 2020; Wen et al., 2019; Yang et al., 1894) Moreover, as MXenes are layered inorganic materials, the bonding between the layers is weak compared to other stacked and van der Waals structured materials. Hence MXenes easily separate into layers when in solution, which reduces the electrode's surface availability and reliability. (Ma et al., 2018) , (Yoon et al., 2016). These disadvantages significantly inhibit the full exploitation of the potential of MXene-based materials. Therefore, it is still a challenge to solve this new material's nanosheets' discrete distribution and aggregation. MWCNTs are usually regarded as the best choice for electrode material because of their high electrical conductivity and readily accessible surface area, which effectively facilitates rapid diffusion and transport of electrolyte ions in the film electrode. (De Volder et al., 2013; Ghosh and Lee, 2012) Given these advantages, MWCNTs with a one-dimensional (1D) structure can provide high conductivity and direct transport paths for carriers by establishing intercalation and "bridging" effect with MXene.(Li et al., 2017). Furthermore, MWCNTs can be successfully inserted into the layers of MXene-$Ti_3C_2T_X$ and connected discrete MXene-$Ti_3C_2T_X$ nanosheets, preventing aggregation. Therefore MWCNT effectively improves the previously mentioned problem of poor electrode ion transport due to the discrete distribution and easy aggregation of MXene. The successful development of this novel hybrid $Ti_3C_2T_X$ - MWCNTs network structure has fully exploited the potential of

MXene-based materials. This hybrid electrode material also provides a multi-dimensional network for transferring charges, thereby increasing the conductivity of the electrode, protecting the electroactive materials, and improving the electrochemical stability. Also, the porous network structure of carbon-based hybrid materials could effectively immobilize the ionophore in the membrane (Samardžić et al., 2017), thus significantly reducing ohmic resistance, shortening the sensor response time, and mitigating noise and signal drift problems in the detection of the condition of low [K^+] concentrations. Figure S1 shows the sensor has low noise and good signal drift suppression characteristics under the condition of low concentration detection. In order to verify the properties and advantages of the fabricated hybrid network structure, the physical and the chemical analyses have been performed using field emission scanning electron microscopy (FESEM), energy dispersive spectrometry (EDS), X-ray photoelectron spectroscopy (XPS), Raman spectroscopy, X-ray diffraction (XRD), Cyclic voltammetry (CV), and Electrochemical impedance spectroscopy (EIS). In order to on-site detect potassium concentration in human sweat, the flexible electrochemical sensor was integrated and assembled with a low-power RF energy harvesting battery-free Near Field Communication (NFC) wireless patch system. The NFC was used to wirelessly transmit measurements to a smartphone and effectively mitigate the problem of commercial lithium-ion batteries, such as their large volume, high energy consumption, and environmental pollution. A microfluidic channel was integrated with the electrochemical sensor patch to efficiently collect sweat on human skin surface and mitigate the sensor surface contamination problem. The accuracy of on-body measurements was verified through the comparison of on-body sensor readings from the arm with ex-situ (off-body) measurements from a PBS with known [K^+] concentration value samples. Figure 1a Shows the conceptual drawing of the operation principle of wireless, battery-free, fully integrated

electrochemical sensing patch based on MWCNTs-MXene hybrid multi-dimensional networks.

2. Material and methods

2.1 Chemicals and instruments

All reagents and apparatus, design of the electrodes are detailed in the supplementary information (S.1).

2.2 Preparation of MXene-Ti_3C2T_x and MWCNTs solutions

$Ti_3C_2T_x$ nanosheets were prepared by etching and exfoliating the MAX phase Ti_3AlC_2 using HCl and LiF. Here, we used (12 M LiF/9 M HCl) with an optimized MILD synthesis method at room temperature. (Alhabeb et al., 2017; Ji et al., 2019; Kalambate et al., 2019) The steps required for MXene synthesis are explained in detail below. First, the etchant was prepared by adding (1 g) LiF to (9 M, 15 mL) HCl and stirring for 10 min. Second, (1 g) of Ti_3AlC_2 powder was added slowly to the etchant and stirred continuously for 24 h at room temperature. Third, the mixture was washed with DI water via centrifugation (5 min per cycle at 4500 rpm) for several cycles. Then, before each centrifugal cycle, the supernatant was poured out, and fresh DI water was added to the precipitate. These washing cycles were repeated until a pH of 6 was achieved. The obtained dark-green precipitate was then combined with DI water and sonicated in an ice bath sonicator for one hour to delaminate the MXene flakes, followed by 12 min centrifugation at 8000 rpm. Finally, the black slurry was carefully collected and dried for 24h in a vacuum at 50 °C, to obtain $Ti_3C_2T_x$ powder. To prepare the MWCNT solution, DMF was selected as the solvent for dispersion. MWCNT powder (24 mg) was weighed with a microbalance and dissolved in 12 mL of DMF dispersant. The mixture was then ultrasonicated at 80 W for 60 min. (Jagadish et al., 2015)

2.3 Design and Fabrication of the Sensor Electrodes

The electrode was successfully fabricated on a flexible PET substrate by screen-printing with a low-cost and low-temperature process. A section of the commercial PET sheet was selected as the substrate, as shown in Figure 1b(I). The PET sheet was cleaned sequentially using isopropyl alcohol (IPA), methanol, and deionized (DI) water. First, the stencil through-hole mask was placed on the substrate PET, as shown in Figure 1b(II). Second, the carbon paste was dropped onto the screen and then rubbed with a squeegee, as shown in Figure 1b(III). Finally, the substrate was separated from the screenprint stencil, as shown in Figure 1b(IV), and the printed carbon electrode was dried at room temperature for 6 h. To assemble the RE for the potentiometric [K^+] sensor, a drop of Ag/AgCl paste was cast onto the carbon/PET electrode and kept at 60° C for 30 min. The silver chloride paste was chosen as a RE material because of its stable potential in electrolyte solutions and to simplify circuit design and system integration.

2.4 Preparation of the [K^+] Sensor

To improve the selectivity, the electrode was coated with valinomycin. Valinomycin is known as a [K^+] selective carrier and inherently has a permeability specific to [K^+], enabling the selective detection of [K^+] by the membrane, which is schematically illustrated in Figure S2 a to e. The [K^+] sensor fabrication process and the [K^+] sensor's structure are shown in Figure 1c. The as-fabricated screen-printed carbon paste electrode was first modified by MXene-$Ti_3C_2T_X$ and then MWCNTs as the transducing layers layer-by-layer manner. (5 µL) of the as-prepared MWCNT solution and (5 µL) of MXene-$Ti_3C_2T_X$ solution were drop-cast on a carbon/PET electrode to increase the catalytic activity and electron transfer rate of the [K^+] sensor, as shown in Figure 1c(I~II). Subsequently, the ion-selective membrane was synthesized as follows. The [K^+]

selective membrane cocktail was composed of (4 mg) of valinomycin, (1 mg) of potassium tetrakis (4-chlorophynyl) borate, (56 mg) of poly(vinyl chloride), and (140 µl) of bis (2-ethylehexyl) sebacate. The cocktail was dissolved in (700 µL) of tetrahydrofuran(Shiwaku et al., 2018). The ion-sensitive alloy was stored in a refrigerator before use. (8 µL) of the as-prepared cocktail was used on the MWCNTs/$Ti_3C_2T_X$-MXene modified carbon electrode, as shown in Figure 1c (III). The [K^+] selective membrane contains valinomycin as a [K^+] transporter, poly (vinyl chloride), and bis (2-ethylehexyl) sebacate as plasticizers and potassium tetrakis (4-chlorophenyl) borate as anion excluder membrane for selective detection of [K^+]. Figure 1c(IV) shows an exploded diagram of the electrode modification material layer-by-layer deposition sequence.

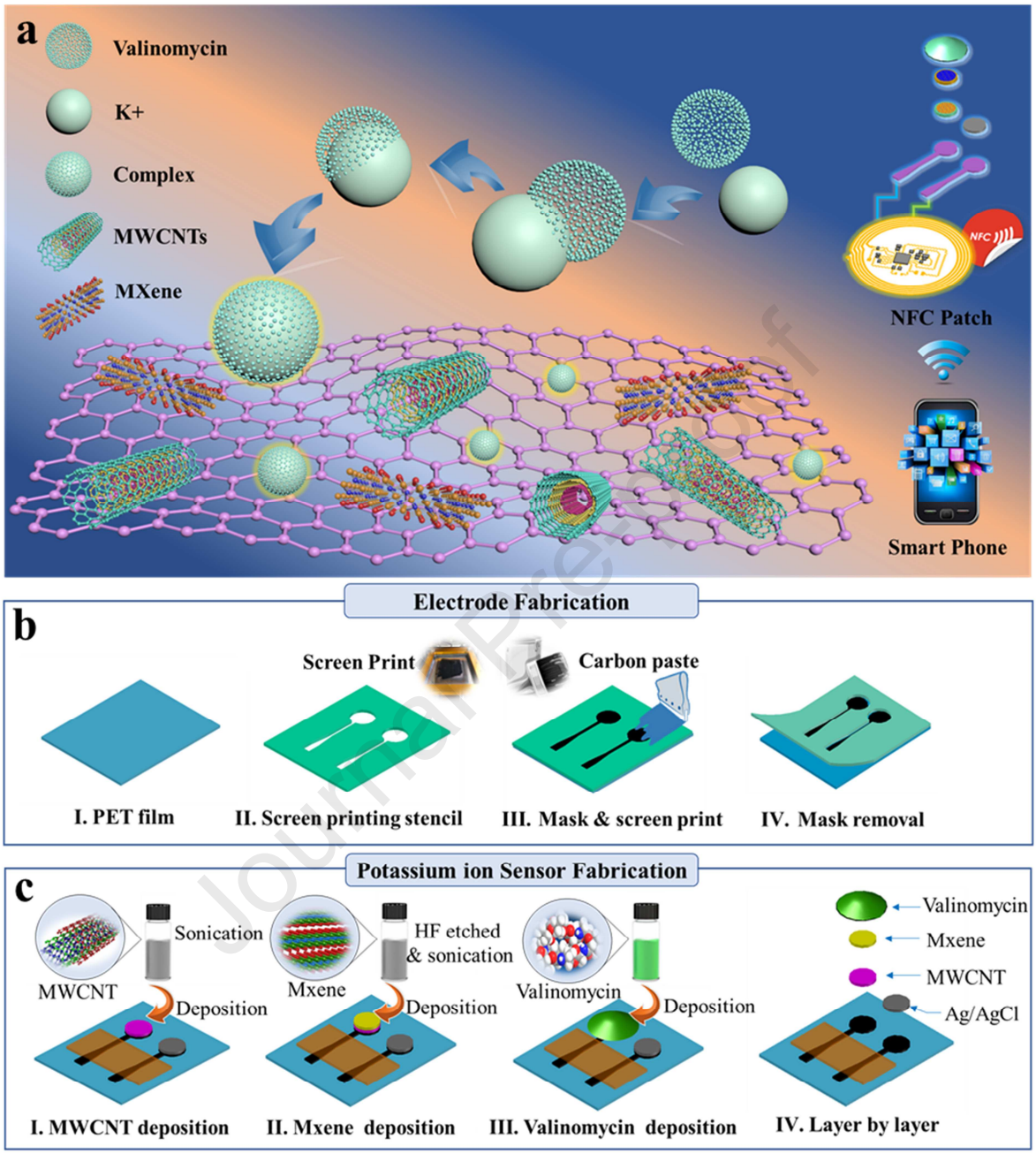

Figure 1. a) Conceptual drawing of the operation principle of wireless, battery-free, fully integrated electrochemical sensing patch based on MWCNTs-MXene hybrid multi-dimensional networks. b) Electrode fabrication steps. c) The [K^+] sensor fabrication steps.

3. Results and discussion

3.1 NFC Electronics and Microfluidics Integrated Systems Design and Analysis

We successfully developed a wireless, battery-free, wearable electrochemical sensing patch system that transmits the [K^+] measurements to a smartphone, as illustrated in the schematic diagram of the system in Figure 2a. The battery-free operation of the sensor patch was accomplished using the radiofrequency electromagnetic energy of the RFID reader. (S. B. Kim et al., 2018; Lin et al., 2020; Zheng et al., 2016) Compared to previous wireless sensor systems, the large battery size issues and massive environmental pollution have been successfully mitigated. The core of an integrated circuit communicates with other modules via a memory data bus and a memory address bus. Instructions and data are sent from the smartphone to the RFID chip through the ISO15693 analog front end and decoded through the ISO15693 decoding module (or coded as it passes RFID to the smartphone). (Dang et al., 2018) The SD14 module of the integrated NFC chip is a multi-channel sigma-delta analog-to-digital converter with up to 14 bits of resolution integrated into the NFC chip consists of a programable gain amplifier (PGA) and a sigma-delta analog-to-digital converter (ADC). The output of the [K^+] sensor was read through a 14-bit ADC convertor. The smartphone application was developed based on an Android studio software program that displays the [K^+] concentration by reading and calibrating the ADC's output voltage. A smartphone was used as an RF power source to activate the developed NFC sensor system wirelessly. When the sensor system is close to the smartphone, it will be identified as NFC-protocol compliant, sent a command to activate the ADC conversions of the rectified voltages, sound a prompt tone to indicate data exchange can begin then, finally, wirelessly transmit the potential value corresponding to the K^+ concentration to the smartphone. In the two-electrode system, the sensor is electrochemically powered and does not require any external

power for its operation. For a [K^+] concentration variation from 1 to 32 mM, the potential output of the sensor between two electrodes varies from 100 mV to 400 mV. The working electrode (WE) was connected to an ADC interface and a reference electrode (RE) to stand voltage (SVSS) in order to enable the virtual ground option SVSS voltage to rise to approximately 125 mV above the ground during ADC sampling. This avoids the small errors caused by the nonlinear behavior of the ADC near the ground. To successfully display the potential range of 100~400 mV performed by the potential [K^+] sensor, the NFC chip was configured to perform cascaded integral comb filtering on the sampled data with an extraction ratio of 256 to achieve noise reduction. During continuous readings of the data, the status register was set to complete the sampling process and data availability. It then reads the FRAM data, converts the ADC value and the corresponding original voltage, then displays it using the pre-calibrated [K^+] concentration value, as shown in Figure S3**.** A PGA is integrated into the SD14 module of the NFC chip. The PGA features a very high-impedance input and a programable gain combined with full offset compensation, very low offset drift, and low noise. The gain of the PGA was selected at SD14GAIN bits. This PGA provides more than 2.8 times the gain of the analog output voltage of the sensor. Hence the sensitivity of the sensor was successfully amplified from 63 to 173 mV/dec, as shown in Figure S4.

Figure 2b shows a photograph of the fabricated four flexible antennas and circuits using photolithography and wet etching of a copper foil coated polyimide film on a silicon wafer. This process is described in detail in the supplementary material, as shown in Figure S5. Figure 2c shows the fabricated ultra-thin (thickness = 32 µm) flexible antenna and circuit. The circuit was soldered using low-temperature solder paste with all the required surface-mounted (SMD)

components. The circuit diagram is shown in Figure S6. The circuits' encapsulation with PDMS protects the NFC electronics from sweat and other external environmental moisture, as shown in Figure 2d. This waterproof design also supports the sensor's operation during water immersion, as shown in Figure S7. To mitigate the problem of sweat collection and surface contamination, we developed a microfluidic system using PDMS and attached it to the sensing system, as shown in Figure 2e. 3D printing technology was used to fabricate the microfluidic mold, which was then filled with liquid PDMS (10:1) and dried for 24 h at 45 °C. Finally, the microfluidic system and the mold were carefully separated. Figure S8a shows the working principle of the designed microfluidic system. It is discussed in detail in the supplementary information S.4. The finite element method's dynamic characteristics of human physiological sweat in the microfluidic device were analyzed, as shown in Figure S8 b,c. The microfluidic chip analysis shows that the dynamic velocity pressure and pressure distribution parameters of human sweat flow in the microfluidic chip are obtained. As a result of the analysis, it is proved that sweat can flow smoothly in the microfluidic, the proposed microfluidic structure shows high-speed flow at the input and output ends, which is conducive to the update of the target detection object, and the detection area (chamber) shows low flow speed, which is conducive to the accurate detection and analysis of the target. Figure 2f shows a very light and small size (diameter = 3.3 cm) circular patch sensor system. Figure 2g shows the wireless NFC sensor and smartphone communication in real-time. Figure 2h shows the block diagram for the complete microfluidic and NFC electronic-based [K^+] monitoring system. Figure 2i shows the real-time monitoring of [K^+] during cycling.

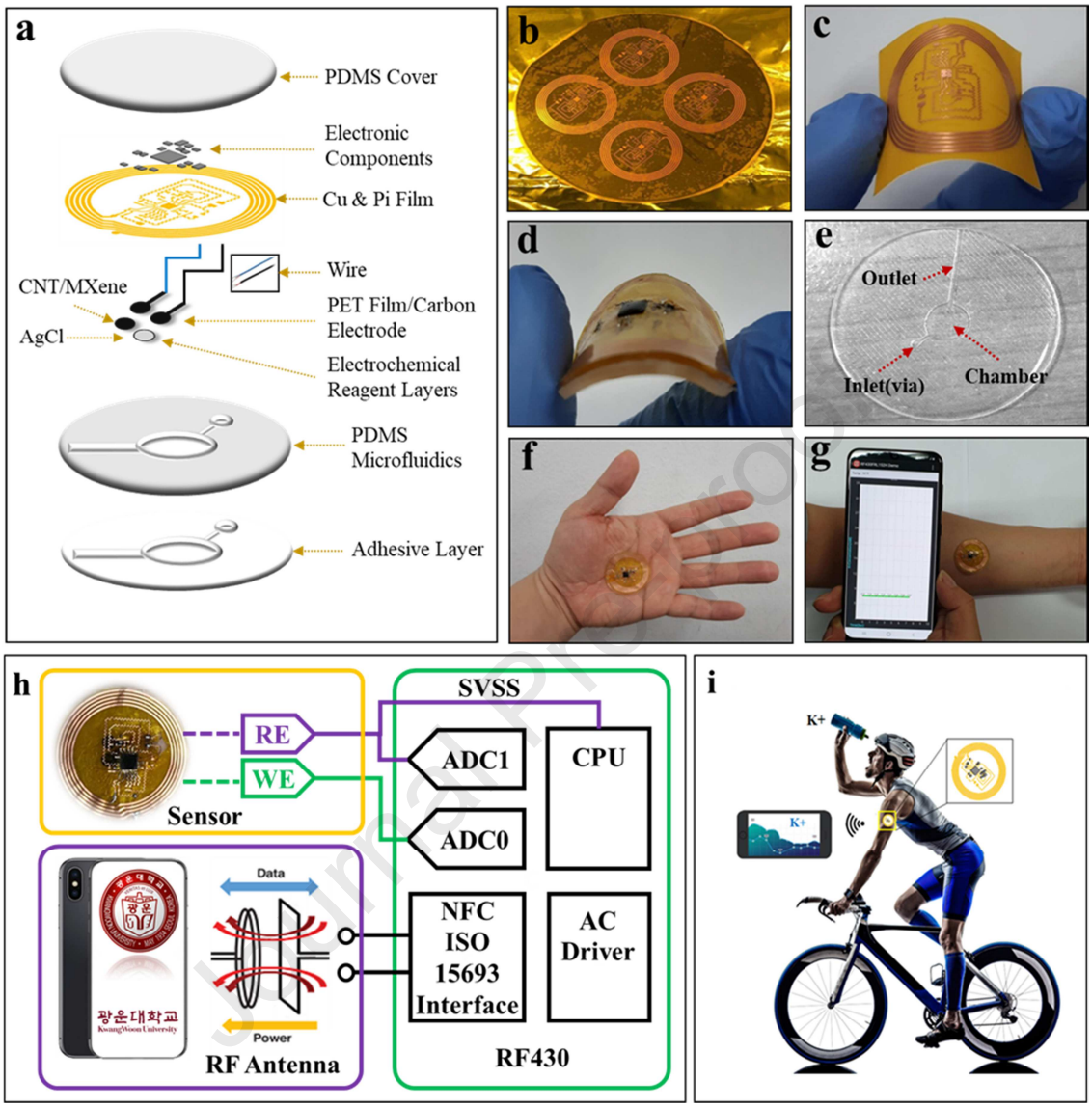

Figure 2. a) Schematic illustrating the exploded view of the wireless, battery-free, flexible, microfluidic/electronic system. b，c) The lithography and etching process is used to make the flexible antenna and circuits. d) Encapsulation of flexible circuits with PDMS. e) The microfluidic system. f) A very light and small size (diameter: 3.3 cm) circular patch sensor system. g) Wireless NFC sensor and smartphone communication in real-time. h) Electronics design, measurement strategy, and complete system. i) Measuring the electrolyte losses from athletes' sweat could help health professionals plan personalized water and electrolyte replacement strategies.

3.2 NFC Electronics Patch Bending and Vertical Distance Test

As seen in Figure S9a, when the sensor patch is curved from the plane, with a 50 – 90 mm curvature, the smartphone can still successfully connect with the sensor patch. The average voltage output of the sensor during bending was 280.1 mV, with a [K^+] concentration of 8 mM, which demonstrates the high precision and reliability of the potential detection. As shown in Figure S9b, when the distance between the smartphone and the patch is less than 20 mm, the voltage output of the NFC chip (power voltage) is stable at approximately 1.97 V. Once the distance exceeds 20 mm, the sensor patch cannot be connected to the smartphone, and the voltage output of the NFC chip reduces to 0 V. Moreover, when the [K^+] sensor was connected to the flexible NFC circuit, and the distance changed periodically between 0 and 20 mm, only small variations in the sensor output were observed with a range of approximately 0.7 mV. This was mainly due to supply voltage fluctuations. Therefore, it is recommended that the smartphone remains close to the sensor patch during detection to avoid such fluctuations.

3.3 Physical Characterization of Fabricated Electrodes

The physical characteristics of the developed electrodes were analyzed by field emission scanning electron microscopy (FESEM), X-ray diffraction (XRD), Raman spectroscopy, and X-ray photoelectron spectroscopy (XPS). FESEM images of the samples, such as bare carbon, carbon/MWCNTs, carbon/MXene, and carbon/MWCNTs/MXene, are shown in Figure 3. The controllable porosity of carbon-based materials can accelerate the kinetic process of ion diffusion of the electrodes. Still, many pinholes exist at the interface of the carbon electrode, as shown in Figure 3a. This is a severe concern for carrier transport, showing a low conductivity. $Ti_3C_2T_X$-MXene, which displays a two-dimensional (2D) layer structure, exhibits very high electrical conductivity and a large surface area (S. J. Kim et al., 2018; Naguib et al., 2011), which

accelerate the carrier transport in the layer. (Liu et al., 2018) However, ultrasonic processing can lead to the formation and crushing of a single $Ti_3C_2T_X$-MXene where the pulverized individual $Ti_3C_2T_X$-MXene sheets agglomerate very easily (Shen et al., 2018) as shown in Figure 3b. which results in a lower conductance of the electrode surface. Figure 3c shows that MWCNTs with a one-dimensional (1D) structure can provide high conductivity and direct transport paths for carriers by establishing an intercalation and "bridging" effect with MXene.(Talib et al., 2018) Simultaneously, MWCNTs were successfully inserted into the carbon pores and between the layered MXene-$Ti_3C_2T_X$ and connected discrete MXene-$Ti_3C_2T_X$ nanosheets because of their linear structure, thereby improving the electrode conductivity effectively, as shown in Figure 3d. This also provides a strong bonding among electrode materials and effectively enhances the electrode's reliability and chemical stability. As a result, we successfully prepared a hybrid network structure of MXene and MWCNTs based on carbon electrodes with very high electrical conductivity and surface areas.

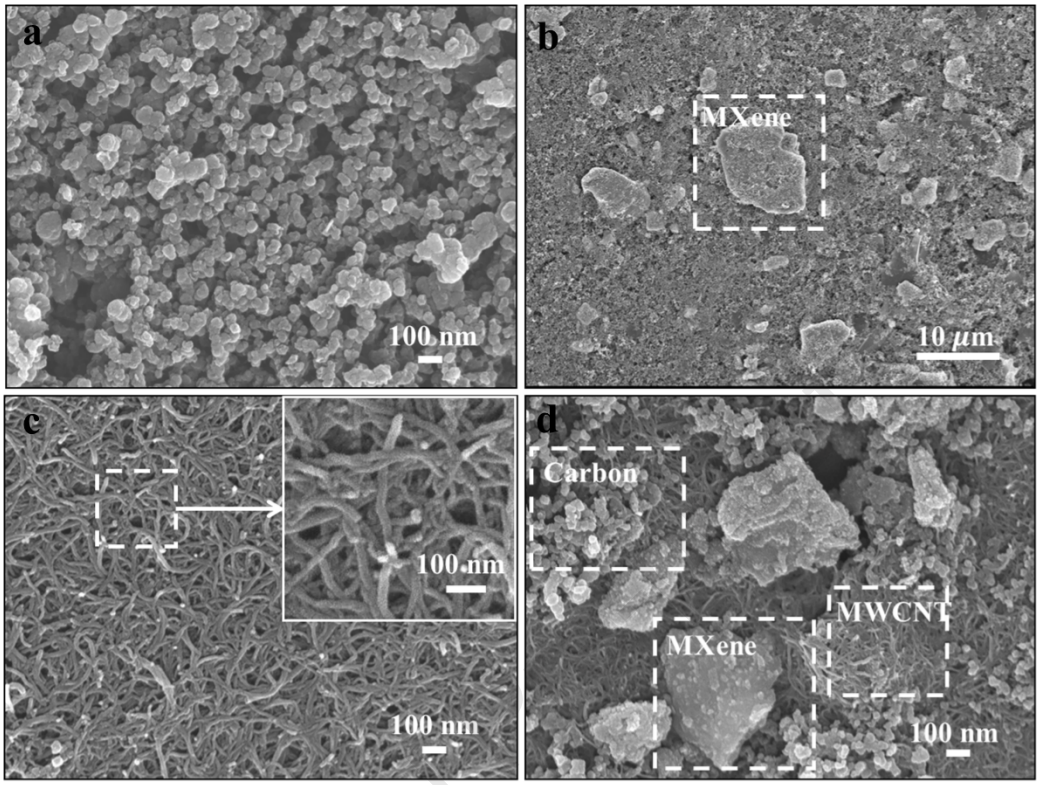

Figure 3. FESEM images of a) Bare Carbon, b) Carbon/MXene-$Ti_3C_2T_x$, c) Carbon/MWCNTs, d) Carbon/MWCNTs/MXene-$Ti_3C_2T_x$.

The chemical structure of MWCNT/MXene hybrid nanosheets was first investigated by XRD and Raman analysis. Figure 4a presents the XRD patterns, indicating the impregnation of a hybrid MXene and MWCNT network into the carbon electrode. The XRD pattern of the carbon/MWCNT composite displays a sharp peak at 26.0° and small peaks at 44.0° and 53.0°, which are assigned to the characteristic (002), (100), and (004) planes, respectively. However, the XRD pattern of the carbon/MWCNTs/MXene composite displays small peaks at 10.0° and 38.0°, which are assigned to the characteristic (002) and (104) planes, respectively. For MXene-$Ti_3C_2T_x$, this confirms the successful synthesis of the hybrid carbon/MWCNTs/MXene nanosheets. As shown in Figure 4b, the Raman spectra show two small bands at around 390 cm^{-1}

and 600 cm^{-1}, designated as the vibrations of atoms in MXene-$Ti_3C_2T_x$. Two other broad bands were detected at approximately 1369 and 1580 cm^{-1}. The former (D-band) corresponds to the disordered graphite caused by defects in a carbon-based material, while the latter (G-band) corresponds to the vibration of sp^2 hybridized carbon atoms in a two-dimensional hexagonal lattice (Xuan et al., 2018; Zahed et al., 2020). The results indicated that the hybrid of MXene and MWCNT network structures was successfully prepared on a commercial carbon paste electrode by this fabrication method. The XPS survey spectrum of the final fabricated electrode is shown in Figure 4c. In the XPS survey region (0 to 800 eV), peaks from the elements C, Ti, and O are well distinguishable for the as-prepared carbon/MWCNT/MXene film. The XPS O1s spectrum reveals the presence of three peaks, which are assigned to C-O (533.7 eV), C=O, and C-Ti-(OH)x (532.7 eV), and C-Ti-Ox (530.9 eV); as shown in Figure 4d.(Weng et al., 2018) The C1s spectrum, shown in Figure 4e, demonstrates the presence of four different peaks, which are attributed to C=C (285.9 eV), C-C (284.6 eV), and COO (289.9 eV) (Rasheed et al., 2018; Wang et al., 2020) The Ti2p spectrum, shown in Figure 4f, reveals the presence of four separate peaks, which are related to Ti-O (465.2 eV) and Ti-C (459.5 eV) (Alizadeh et al., 2018; Cai et al., 2018; Zhao et al., 2019). Furthermore, the elemental composition of the developed platform (Carbon/MWCNTs/MXene) was carefully investigated through EDS mapping, as shown in Figure S10. The atomic percentages of C, O, and Ti were mapped as 84.76%, 8.11%, and 7.13%, respectively, in agreement with the XPS results. The results show the successful preparation of the hybrid structure of MXene and MWCNTs based on carbon electrodes.

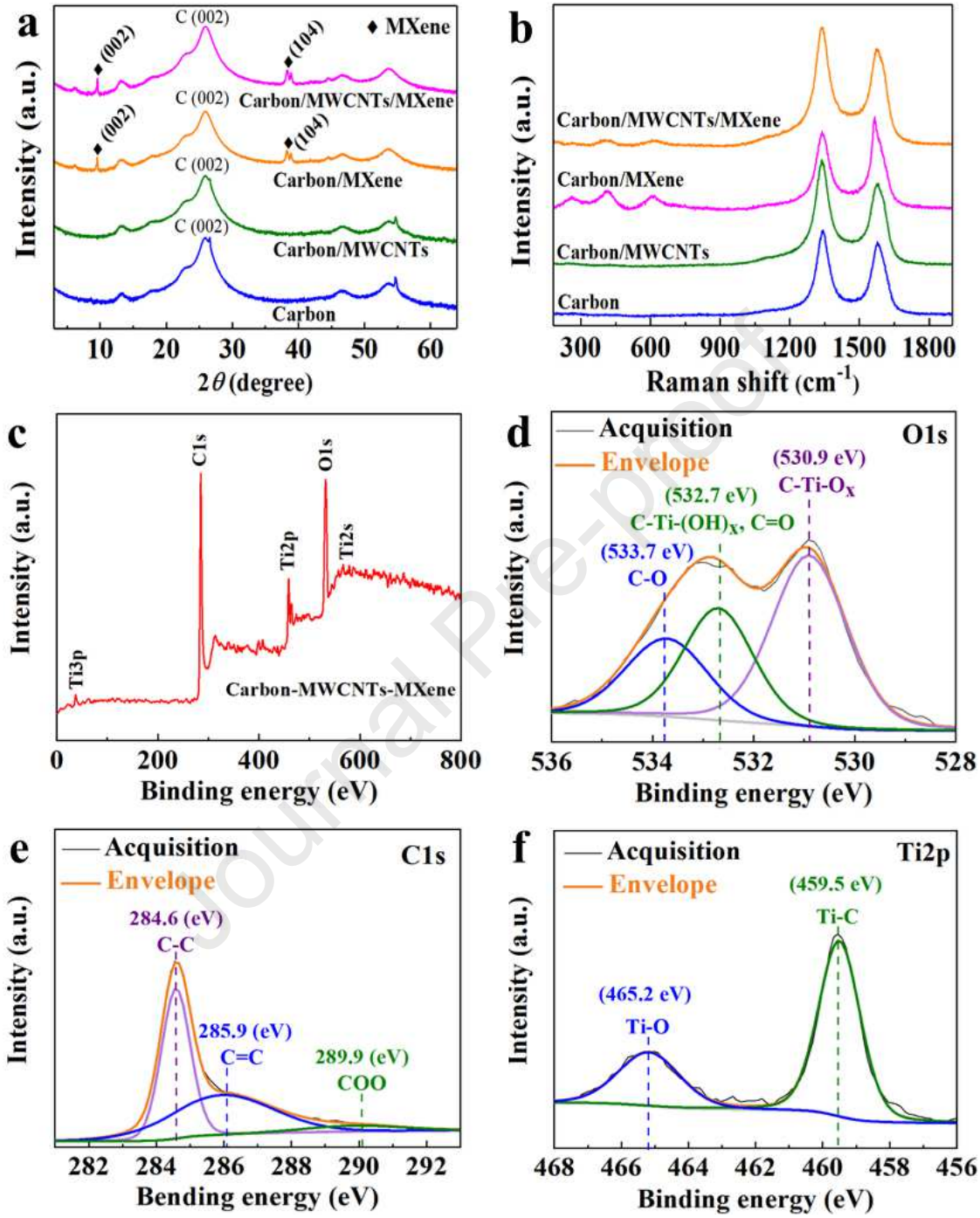

Figure 4. a) XRD spectrum of the carbon/MWCNT/MXene composite films. b) Raman spectrum of the carbon/MWCNT/MXene composite films. c) XPS survey spectrum of the carbon/MWCNT/MXene composite films. d) High-resolution XPS spectra of the O1s region. e) C1s region. f) Ti2p region.

3.4 Electrochemical Characterization of Fabricated Electrodes

The catalytic activities and interfacial properties of the developed electrodes were investigated by cyclic voltammetry (CV) and electrochemical impedance (EIS) measurements, as shown in Figure 5. As shown in Figure 5a, displays CV of MWCNTs, $Ti_3C_2T_x$, and MWCNTs/$Ti_3C_2T_x$ modified Carbon/PET electrodes in 5 mM [Fe(CN)6] $^{3-/4-}$ containing 0.1 M KCl at the scan rate of 50 mV s^{-1}. The CV area of the carbon/MWCNTs/MXene electrode was higher than that of the bare carbon, carbon/MWCNTs, and carbon/MXene electrode, indicating superior electrocatalytic activity. By used EIS analyzed the interface performance of the modified electrode. Figure 5b presents the EIS spectra of the various modified electrodes, bare carbon, carbon/MWCNTs, carbon/MXene, and carbon/MWCNTs/MXene, tested using a 5 mM $Fe(CN)_6^{3-/4-}$ redox probe. The inset figure shows the Randles equivalent circuit model used to fit the experimental results. The electron transfer resistance (R_{ct}) values for bare carbon, carbon/MWCNTs, carbon/MXene, and carbon/MWCNTs/MXene electrodes are approximate ~3.8 kΩ, ~3.4 kΩ, ~611Ω, and ~203 Ω, respectively. The low R_{ct} value obtained for the carbon/MWCNTs/MXene electrode implies superior electron transfer properties than the carbon/MXene electrode. Cyclic voltammetry was further utilized (scan rate range of 25–200 mV s^{-1}) to investigating the diffusion controlled process of the redox probe on the carbon/MWCNTs/MXene electrode shown in Figure 5c. The peak current of oxidation and reduction both increased with increasing scanning rates. Figure 5d showed an excellent linear relationship with the square root of the scanning rate.

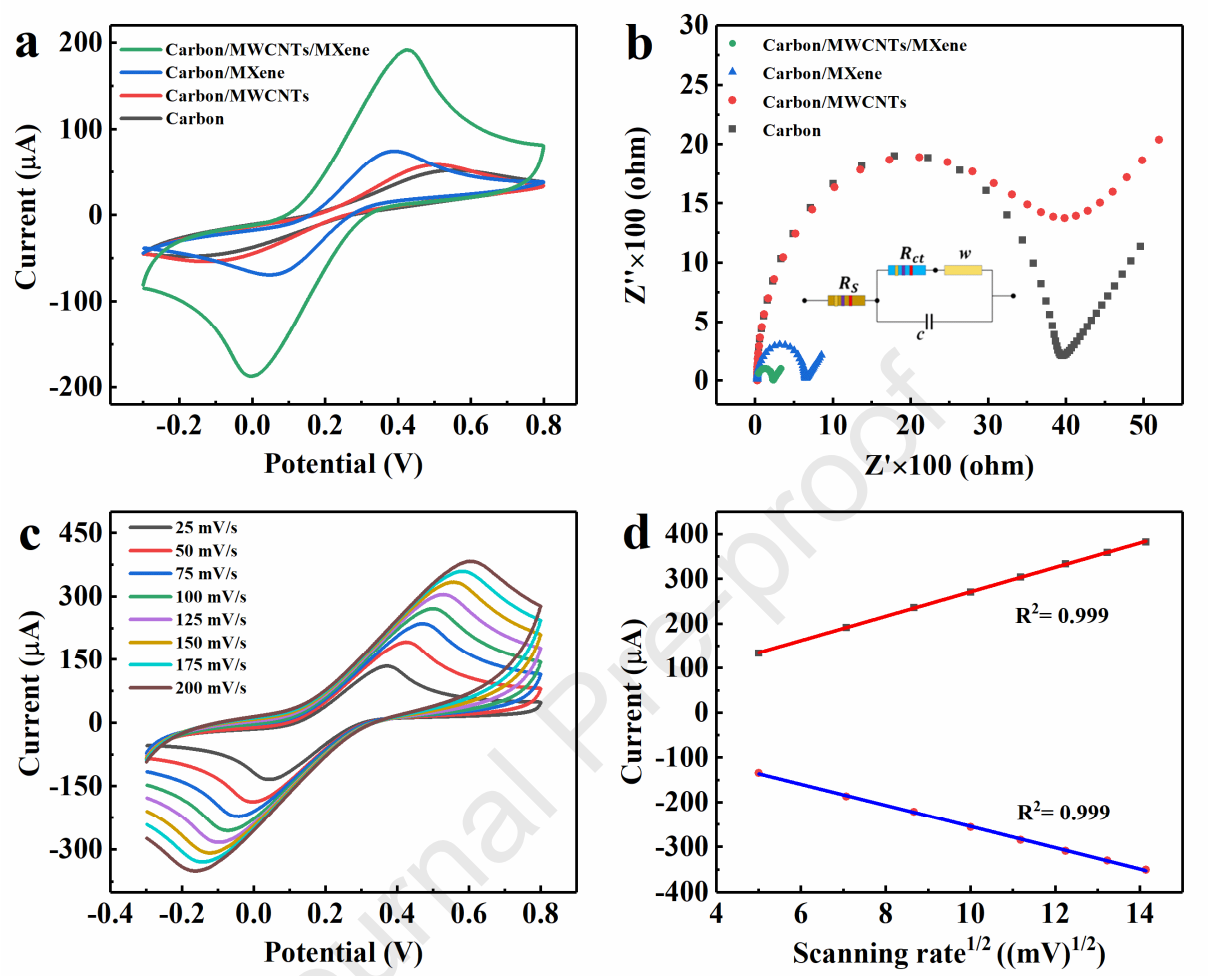

Figure 5. a) CV performance analysis of bare carbon, carbon/MWCNTs, carbon/MXene, and carbon/MWCNTs/MXene. b) EIS fitted curves of bare carbon, carbon/MWCNTs, carbon/MXene, and carbon/MWCNTs/MXene (The inset shows the equivalent circuit used in fitting). c) Diffusion controlled process for carbon/MWCNTs/MXene modified electrode, and d) corresponding calibration curve.

3.5 Electrochemical Investigation of the [K^+] Sensor

The determination of [K^+] was investigated using the potentiometric method. The ion-selective electrode (ISE) potential changes gradually over a few seconds when [K^+] is added. The potential at different concentrations is stable at a constant value, which allows quantitative measurements of the [K^+] level, as shown in Figure 6a. Figure 6b shows the calibration plot for the sensor as a

function of [K^+] concentration, extracted from Figure 6a. The total potential change was 95 mV when the [K^+] concentration changed from 1 to 32 mM, which resulted in a sensitivity of 63 mV/dec. We estimated the response time by changing the concentration of [K^+] in the solution, and the sensor exhibited a fast response time of 2 s, as shown in Figure 6c. Human sweat also contains other primary chemical ions (Ca^{2+}, Na^+, Zn^{2+}). Therefore, the sensor interference response was also investigated. The selectivity experiment of the sensor was carried out using the potential response method. Compared to the signals of the [K^+] droplets, the results did not present any significant interference signals, indicating that the sensor exhibits excellent selectivity for [K^+], as shown in Figure 6d. Additionally, the sensors should be reproducible so that reliable analysis can be obtained from individual sensors. Figure 6e shows the reproducibility experiment of five different sensors, which were tested in a solution containing a 1−32 mM [K^+] concentration ranging from 398.6 to 514.3 mV in the presence of 1 mM [K^+]. The repeatability of each sensor was evaluated systematically, and several potential response experiments were carried out ten times, as shown in Figure 6f. These results show that the [K^+] sensor has good repeatability and reproducibility. The [K^+] sensor designed in this study was compared with the performance of alternative sensors detailed in published scientific literature and are tabulated in Table S2. By comparison with other [K^+] sensors, it was observed that the carbon/MWCNTs/MXene composite sensor exhibited a very high sensitivity within the clinical range of [K^+] in sweat.

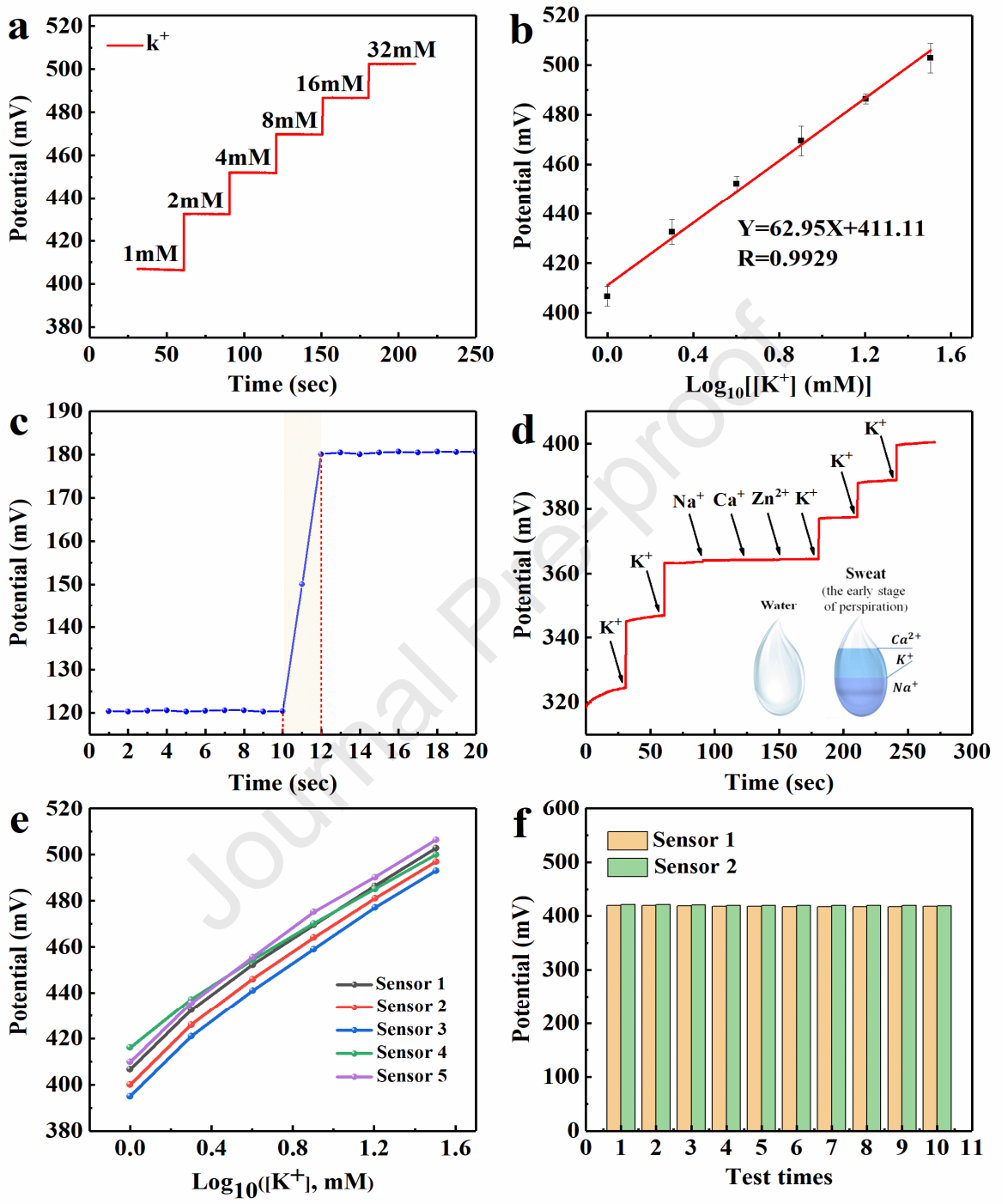

Figure 6. a) Potentiometric response for [K^+] ISE. b) Evaluation of the linear range. c) The response time of the sensor. d) The selectivity experiment of the sensor carried out by the potential response method with successive addition of 1 mM [K^+] (two-fold), followed by

electroactive interfering species of 20-μM Zn^{2+}, 4 mM Na^{+}, and 4 mM Ca^{2+}; and finally; 8 mM, 16 mM, and 32 mM [K^{+}] in 0.05 M phosphate buffer solution (PBS) (pH = 7.4). e) The reproducibility test with five sensors. f) The repeatability analysis of the sensor evaluated systematically by observing the potential response of two sensors on ten separate occasions.

3.6 Real-time Monitoring of [K^{+}] Concentration Levels in the Human Body

The accuracy of on-body measurements was verified through the comparison of on-body sensor readings from the arm with ex-situ (off-body) measurements from a PBS with known [K^{+}] concentration value samples, as shown in Figure S11a. The known concentrations of [K^{+}] were diluted in a 0.1 M PBS and used for calibration. First, the NFC wireless system was connected to the electrochemical [K^{+}] sensor, which was immersed in a PBS. The smartphone was connected to the PC, using the pre-installed application to activate the Android studio software program when the smartphone was close to the NFC system. Simultaneously, the Android studio software program on the PC displays the sensor's real-time output potential. Finally, the voltage level of a PBS with known [K^{+}] concentration values (1, 2,4, 8, 16, 32 mM) was used for calibration, as shown in Figure S3. The relationship between the voltage and [K^{+}] concentration of the test solution was estimated based on calibration with a standard buffer solution. The data are read from the FRAM, with the ADC values and corresponding raw voltages converted and displayed as [K^{+}] concentration values using pre-calibration. The developed flexible NFC patch [K^{+}] sensor can be worn comfortably on the arm. Figure S11b shows a human subject wearing the flexible NFC patch [K^{+}] sensor, allowing for real-time perspiration monitoring on the arm during cycling. To ensure the fidelity of sensor readings, data collection occurred only when a sufficient sweat sample was present in the microfluidic channel. Finally, the feasibility of the fabricated sensor and NFC wireless electrochemical sensing patch is verified by comparing the results of

the standard addition method of diluted human perspiration samples, as depicted in Table S1. The specific methods are discussed in detail in the supplementary information S.6.

4. Conclusions

In this work, we have successfully developed a high-performance MWCNTs/MXene-$Ti_3C_2T_X$ based wireless, battery-free, wearable, and microfluidic smart electrochemical system for detecting [K^+] in human sweat. The results demonstrated that the "bridging" effect of carbon/MWCNTs/MXene is conducive to the electron transmission of catalyst carriers and thus improves the electrocatalytic performance of the [K^+] sensor. In addition, the appearance of MWCNTs and $Ti_3C_2T_X$-MXene can enhance surface contact with carbon paste and promote electrode conductivity. The porous network structure of carbon-based hybrid materials effectively immobilizes the ionophore in the membrane, thus significantly reducing ohmic resistance, shortening the sensor response time, and mitigating the noise and signal drift issues with low [K^+] concentration detection. The fabricated sensor measured the [K^+] concentration of human sweat with a high sensitivity of 63 mV/dec, which was successfully amplified to 173 mV/dec using an NFC amplification system with a high linear range from 1 to 32 mM. The feasibility of the system was confirmed by collecting sweat using the microfluidic system and measuring [K^+] in human sweat instantaneously. Simultaneously, a smartphone was used as an RF power source to wirelessly activate NFC electronic systems and receive sensing data from the device, using a smartphone application developed based on an Android studio software program displaying the detection [K^+] concentration values.

Acknowledgments

This work was supported by the Technology Innovation Program (20000773, Development of

nano multi-sensors based on wearable patch for non-hematological monitoring of metabolic syndrom) funded by the Ministry of Trade, Industry & Energy (MI, Korea), the Bio & Medical Technology Development Program of the NRF grant funded by the Korean government (MSIT) (NRF- 2017M3A9F1031270), and by the Research Grant of Kwangwoon University in 2018. The authors are also grateful to the members of the ASER group for their technical support.

References

Alhabeb, M., Maleski, K., Anasori, B., Lelyukh, P., Clark, L., Sin, S., Gogotsi, Y., 2017. Guidelines for Synthesis and Processing of Two-Dimensional Titanium Carbide (Ti3C2Tx MXene). Chem. Mater. 29, 7633–7644. https://doi.org/10.1021/acs.chemmater.7b02847

Alizadeh, A., Burns, A., Lenigk, R., Gettings, R., Ashe, J., Porter, A., McCaul, M., Barrett, R., Diamond, D., White, P., Skeath, P., Tomczak, M., 2018. A wearable patch for continuous monitoring of sweat electrolytes during exertion. Lab Chip 18, 2632–2641. https://doi.org/10.1039/c8lc00510a

Baker, L.B., Ungaro, C.T., Barnes, K.A., Nuccio, R.P., Reimel, A.J., Stofan, J.R., 2014. Validity and reliability of a field technique for sweat Na+ and K+ analysis during exercise in a hot-humid environment. Physiol. Rep. 2. https://doi.org/10.14814/phy2.12007

Barnes, K.A., Anderson, M.L., Stofan, J.R., Dalrymple, K.J., Reimel, A.J., Roberts, T.J., Randell, R.K., Ungaro, C.T., Baker, L.B., 2019. Normative data for sweating rate, sweat sodium concentration, and sweat sodium loss in athletes: An update and analysis by sport. J. Sports Sci. 37, 2356–2366. https://doi.org/10.1080/02640414.2019.1633159

Bobacka, J., Ivaska, A., Lewenstam, A., 1999. Plasticizer-free all-solid-state potassium-selective

electrode based on poly (3-octylthiophene) and valinomycin 385, 195–202.

Cai, Y., Shen, J., Ge, G., Zhang, Y., Jin, W., Huang, W., Shao, J., Yang, J., Dong, X., 2018. Stretchable Ti3C2Tx MXene/Carbon Nanotube Composite Based Strain Sensor with Ultrahigh Sensitivity and Tunable Sensing Range. ACS Nano 12, 56–62. https://doi.org/10.1021/acsnano.7b06251

Dang, W., Manjakkal, L., Navaraj, W.T., Lorenzelli, L., 2018. Biosensors and Bioelectronics Stretchable wireless system for sweat pH monitoring. Biosens. Bioelectron. 107, 192–202. https://doi.org/10.1016/j.bios.2018.02.025

De Volder, M.F.L., Tawfick, S.H., Baughman, R.H., Hart, A.J., 2013. Carbon nanotubes: Present and future commercial applications. Science (80-.). 339, 535–539. https://doi.org/10.1126/science.1222453

Fan, X., Li, H., Zhao, J., Lin, F., Zhang, L., Zhang, Y., Yao, S., 2012. A novel label-free fluorescent sensor for the detection of potassium ion based on DNAzyme. Talanta 89, 57–62. https://doi.org/10.1016/j.talanta.2011.11.056

Gao, W., Emaminejad, S., Nyein, H.Y.Y., Challa, S., Chen, K., Peck, A., Fahad, H.M., Ota, H., Shiraki, H., Kiriya, D., Lien, D.H., Brooks, G.A., Davis, R.W., Javey, A., 2016. Fully integrated wearable sensor arrays for multiplexed in situ perspiration analysis. Nature 529, 509–514. https://doi.org/10.1038/nature16521

Ghosh, A., Lee, Y.H., 2012. Carbon-based electrochemical capacitors. ChemSusChem 5, 480–499. https://doi.org/10.1002/cssc.201100645

Jagadish, K., Srikantaswamy, S., Byrappa, K., Shruthi, L., Abhilash, M.R., 2015. Dispersion of Multiwall Carbon Nanotubes in Organic Solvents through Hydrothermal Supercritical Condition. J. Nanomater. 2015. https://doi.org/10.1155/2015/381275

Ji, J., Zhao, L., Shen, Y., Liu, S., Zhang, Y., 2019. Covalent stabilization and functionalization of MXene via silylation reactions with improved surface properties. FlatChem 17, 100128. https://doi.org/10.1016/j.flatc.2019.100128

Kalambate, P.K., Gadhari, N.S., Li, X., Rao, Z., Navale, S.T., Shen, Y., Patil, V.R., Huang, Y., 2019. Recent advances in MXene–based electrochemical sensors and biosensors. TrAC - Trends Anal. Chem. 120, 115643. https://doi.org/10.1016/j.trac.2019.115643

Kim, S.B., Lee, K.H., Raj, M.S., Lee, B., Reeder, J.T., Koo, J., Hourlier-Fargette, A., Bandodkar, A.J., Won, S.M., Sekine, Y., Choi, J., Zhang, Y., Yoon, J., Kim, B.H., Yun, Y., Lee, S., Shin, J., Kim, J., Ghaffari, R., Rogers, J.A., 2018. Soft, Skin-Interfaced Microfluidic Systems with Wireless, Battery-Free Electronics for Digital, Real-Time Tracking of Sweat Loss and Electrolyte Composition. Small 14, 1–9. https://doi.org/10.1002/smll.201802876

Kim, S.J., Koh, H.J., Ren, C.E., Kwon, O., Maleski, K., Cho, S.Y., Anasori, B., Kim, C.K., Choi, Y.K., Kim, J., Gogotsi, Y., Jung, H.T., 2018. Metallic Ti3C2Tx MXene Gas Sensors with Ultrahigh Signal-to-Noise Ratio. ACS Nano 12, 986–993. https://doi.org/10.1021/acsnano.7b07460

Li, X., Yin, X., Han, M., Song, C., Xu, H., Hou, Z., Zhang, L., Cheng, L., 2017. Ti3C2 MXenes modified with: In situ grown carbon nanotubes for enhanced electromagnetic wave absorption properties. J. Mater. Chem. C 5, 4068–4074. https://doi.org/10.1039/c6tc05226f

Lin, R., Kim, H.J., Achavananthadith, S., Kurt, S.A., Tan, S.C.C., Yao, H., Tee, B.C.K., Lee, J.K.W., Ho, J.S., 2020. Wireless battery-free body sensor networks using near-field-enabled clothing. Nat. Commun. 11, 1–10. https://doi.org/10.1038/s41467-020-14311-2

Liu, D., Wang, R., Chang, W., Zhang, L., Peng, B., Li, H., Liu, S., Yan, M., Guo, C., 2018. Ti3C2 MXene as an excellent anode material for high-performance microbial fuel cells. J. Mater. Chem. A 6, 20887–20895. https://doi.org/10.1039/c8ta07305h

Ma, Z., Zhou, X., Deng, W., Lei, D., Liu, Z., 2018. 3D Porous MXene (Ti3C2)/Reduced Graphene Oxide Hybrid Films for Advanced Lithium Storage. ACS Appl. Mater. Interfaces 10, 3634–3643. https://doi.org/10.1021/acsami.7b17386

Naguib, M., Kurtoglu, M., Presser, V., Lu, J., Niu, J., Heon, M., Hultman, L., Gogotsi, Y., Barsoum, M.W., 2011. Two-dimensional nanocrystals produced by exfoliation of Ti 3AlC 2. Adv. Mater. 23, 4248–4253. https://doi.org/10.1002/adma.201102306

Orangi, J., Hamade, F., Davis, V.A., Beidaghi, M., 2020. 3D Printing of Additive-Free 2D Ti3C2Tx (MXene) Ink for Fabrication of Micro-Supercapacitors with Ultra-High Energy Densities. ACS Nano 14, 640–650. https://doi.org/10.1021/acsnano.9b07325

Rasheed, P.A., Pandey, R.P., Rasool, K., Mahmoud, K.A., 2018. Ultra-sensitive electrocatalytic detection of bromate in drinking water based on Nafion/Ti3C2Tx (MXene) modified glassy carbon electrode. Sensors Actuators, B Chem. 265, 652–659. https://doi.org/10.1016/j.snb.2018.03.103

Samardžić, M., Galović, O., Hajduković, M., Sak-Bosnar, M., 2017. A novel, fast responding, low noise potentiometric sensor containing a carbon-based polymeric membrane for

measuring surfactants in industrial and environmental applications. Talanta 162, 316–323. https://doi.org/10.1016/j.talanta.2016.10.041

Shen, C., Wang, L., Zhou, A., Wang, B., Wang, X., Lian, W., Hu, Q., Qin, G., Liu, X., 2018. Synthesis and electrochemical properties of two-dimensional RGO/Ti3 C2 Tx nanocomposites. Nanomaterials 8, 1–11. https://doi.org/10.3390/nano8020080

Shiwaku, R., Matsui, H., Nagamine, K., Uematsu, M., Mano, T., Nomura, A., Tsuchiya, K., Hayasaka, K., Takeda, Y., 2018. OPEN A Printed Organic Amplification System for Wearable Potentiometric Electrochemical Sensors. Sci. Rep. 1–8. https://doi.org/10.1038/s41598-018-22265-1

Sonner, Z., Wilder, E., Heikenfeld, J., Kasting, G., Beyette, F., Swaile, D., Sherman, F., Joyce, J., Hagen, J., Kelley-Loughnane, N., Naik, R., 2015. The microfluidics of the eccrine sweat gland, including biomarker partitioning, transport, and biosensing implications. Biomicrofluidics 9. https://doi.org/10.1063/1.4921039

Talib, N.A.A., Salam, F., Yusof, N.A., Alang Ahmad, S.A., Azid, M.Z., Mirad, R., Sulaiman, Y., 2018. Enhancing a clenbuterol immunosensor based on poly(3,4-ethylenedioxythiophene)/multi-walled carbon nanotube performance using response surface methodology. RSC Adv. 8, 15522–15532. https://doi.org/10.1039/c8ra00109j

Teixeira, M.F.S., Freitas, B.H., Seraphim, P.M., Salmazo, L.O., Nobre, M.A., Lanfredi, S., 2009. Development of an electrochemical sensor for potassium ions based on KSr2Nb5O15 modified electrode. Procedia Chem. 1, 293–296. https://doi.org/10.1016/j.proche.2009.07.073

Viera, A.J., Wouk, N., 2015. Potassium disorders: Hypokalemia and hyperkalemia. Am. Fam. Physician 92, 487–495.

Villiger, M., Stoop, R., Vetsch, T., Hohenauer, E., Pini, M., Clarys, P., Pereira, F., Clijsen, R., 2018. Evaluation and review of body fluids saliva, sweat and tear compared to biochemical hydration assessment markers within blood and urine. Eur. J. Clin. Nutr. 72, 69–76. https://doi.org/10.1038/ejcn.2017.136

Wang, J., Zhang, Z., Yan, X., Zhang, S., Wu, Z., Zhuang, Z., Han, W.Q., 2020. Rational Design of Porous N-Ti3C2 MXene@CNT Microspheres for High Cycling Stability in Li–S Battery. Nano-Micro Lett. 12. https://doi.org/10.1007/s40820-019-0341-6

Wen, Y., Ma, C., Wei, Z., Zhu, X., Li, Z., 2019. FeNC/MXene hybrid nanosheet as an efficient electrocatalyst for oxygen reduction reaction. RSC Adv. 9, 13424–13430. https://doi.org/10.1039/c9ra01330j

Weng, G., Li, J., Alhabeb, M., Wang, H., Lipton, J., Maleski, K., Kong, J., Shaulsky, E., Elimelech, M., Taylor, A.D., Maleski, K., Kong, J., Shaulsky, E., Elimelech, M., 2018. Layer-by-Layer Assembly of Cross-Functional Semi- transparent MXene-Carbon Nanotubes Composite Films for Next-Generation Electromagnetic Interference Shielding. https://doi.org/10.1002/adfm.201803360

Xuan, X., Yoon, H.S., Park, J.Y., 2018. A wearable electrochemical glucose sensor based on simple and low-cost fabrication supported micro-patterned reduced graphene oxide nanocomposite electrode on flexible substrate. Biosens. Bioelectron. 109, 75–82. https://doi.org/10.1016/j.bios.2018.02.054

Yang, B., She, Y., Zhang, C., Kang, S., Zhou, J., Hu, W., 1894. Nitrogen Doped Intercalation TiO 2 / TiN / Ti 3 C 2 T x Nanocomposite Electrodes with Enhanced Pseudocapacitance.

Yoon, J.H., Park, H.J., Park, S.H., Lee, K.G., Choi, B.G., 2020. Electrochemical characterization of reduced graphene oxide as an ion-to-electron transducer and application of screen-printed all-solid-state potassium ion sensors. Carbon Lett. 30, 73–80. https://doi.org/10.1007/s42823-019-00072-6

Yoon, Y., Lee, K., Lee, H., 2016. Low-dimensional carbon and MXene-based electrochemical capacitor electrodes. Nanotechnology 27. https://doi.org/10.1088/0957-4484/27/17/172001

Yuan, Q., Wu, S., Ye, C., Liu, X., Gao, J., Cui, N., Guo, P., Lai, G., Wei, Q., Yang, M., Su, W., Li, H., Jiang, N., Fu, L., Dai, D., Lin, C. Te, Chee, K.W.A., 2019. Sensitivity enhancement of potassium ion (K+) detection based on graphene field-effect transistors with surface plasma pretreatment. Sensors Actuators, B Chem. 285, 333–340. https://doi.org/10.1016/j.snb.2019.01.058

Zahed, M.A., Barman, S.C., Das, P.S., Sharifuzzaman, M., Yoon, H.S., Yoon, S.H., Park, J.Y., 2020. Highly flexible and conductive poly (3, 4-ethylene dioxythiophene)-poly (styrene sulfonate) anchored 3-dimensional porous graphene network-based electrochemical biosensor for glucose and pH detection in human perspiration. Biosens. Bioelectron. 160. https://doi.org/10.1016/j.bios.2020.112220

Zeng, X., Qin, W., 2017. A solid-contact potassium-selective electrode with MoO2 microspheres as ion-to-electron transducer. Anal. Chim. Acta 982, 72–77. https://doi.org/10.1016/j.aca.2017.05.032

Zhao, L., Wang, K., Wei, W., Wang, L., Han, W., 2019. High-performance flexible sensing devices based on polyaniline/MXene nanocomposites. InfoMat 1, 407–416. https://doi.org/10.1002/inf2.12032

Zheng, Q., Zhang, H., Shi, B., Xue, X., Liu, Z., Jin, Y., Ma, Y., Zou, Y., Wang, X., An, Z., Tang, W., Zhang, W., Yang, F., Liu, Y., Lang, X., Xu, Z., Li, Z., Wang, Z.L., 2016. In Vivo Self-Powered Wireless Cardiac Monitoring via Implantable Triboelectric Nanogenerator. ACS Nano 10, 6510–6518. https://doi.org/10.1021/acsnano.6b02693

Highlight

- An ultra-high sensitive, flexible, wireless, battery-free, wireless RF energy harvesting, fully integrated electrochemical sensing patch, including a microfluidic-sweat collecting unit.
- On-site monitoring [K^+] concentration in human perspiration.
- MWCNTs-MXene hybrid multi-dimensional networks obtain a high surface activation area and faster charge transfer rate, strongly adsorbing the valinomycin membrane to protect ionophore for effective transshipment and immobilization [K^+].

Declaration of interests

√ The authors declare that they have no known competing financial interests or personal relationships that could have appeared to influence the work reported in this paper.

☐The authors declare the following financial interests/personal relationships which may be considered as potential competing interests:

N/A